Curvature and strain effects on electronic properties of single-wall carbon nanotubes

2003 J. Phys.: Condens. Matter 15 L439

(http://iopscience.iop.org/0953-8984/15/27/101)

INSTITUTE OF PHYSICS PUBLISHING JOURNAL OF PHYSICS: CONDENSED MATTER

J. Phys.: Condens. Matter **15** (2003) L439–L445 PII: S0953-8984(03)63828-2

LETTER TO THE EDITOR

Curvature and strain effects on electronic properties of single-wall carbon nanotubes

J W Ding[1,2], X H Yan[1], J X Cao[1,2], D L Wang[1,2], Y Tang[1] and Q B Yang[1]

[1] Department of Physics, Xiangtan University, Xiangtan 411105, Hunan, People's Republic of China
[2] Institute of Mechanics and Material Engineering, Xiangtan University, Xiangtan 411105, Hunan, People's Republic of China

E-mail: jwding@xtu.edu.cn

Received 23 May 2003
Published 27 June 2003
Online at stacks.iop.org/JPhysCM/15/L439

Abstract

To describe accurately the electronic structures of carbon nanotubes, a semi-empirical tight-binding approach is presented in which the main intrinsic curvatures have been fully taken into account. The calculated electronic structures and band gaps are consistent with experimental measurements. Studies of the relative importance of various intrinsic curvatures show that each curvature has a contribution of varying importance to the curvature-induced band gap. Additionally, under both uniaxial and torsional strain, semiconductor–metal–semiconductor phase transitions have been observed for primary metallic carbon nanotubes. The critical stress of the transition and the gap's sensitivity with stress are dependent on both the diameter and chirality of nanotubes, which is at variance with previous predictions.

While rolling a graphite sheet into a single-wall carbon nanotube (SWCN), the curvature leads to hybridization of the graphitic σ- and π-states and modifies both the length and angle of bonds between two nearest-neighbouring carbon atomic orbitals. Using both *ab initio* calculations and a tight-binding sp^3 approach, Blase *et al* [1] showed that only the σ–π hybridization effect may dramatically change the band structures of SWCNs. Kleiner *et al* [2] studied analytically the curvature hybridization. A curvature-induced gap of the order of $1/D^2$ was obtained in primary metallic SWCNs with tube diameter D. The ultraviolet photoemission spectroscopy He II spectral measurement [3] provided further evidence of the σ–π hybridization effect in the SWCNs. Also, assuming that the transfer integrals γ_i are proportional to the cosine of the misalignment angle, a scaling law of band gaps with D^{-2} dependence has also been obtained using a single-π orbital model for these nanotubes [4–6], which fits well with the experimental data [6–9]. Additionally, in terms of the Harrison formula [10], the bond-length modified transfer integrals were re-calculated to study the response of the electronic properties

to strain [11–13]. It is found that the electronic properties of SWCNs are sensitive to the variations in bond length. These results show that each type of intrinsic curvature is responsible for the curvature-induced band gap in a SWCN. How does a combination of these main intrinsic curvatures affect the electronic properties of the nanotubes? Here, we present the details of a sp^3 tight-binding approach for including the main intrinsic curvatures. The curvature effects and their relative importance have been explored. Additionally, the SWCNs that were studied may be subject to various mechanical deformations in the process of both the preparation and the measurement [14–18], which may alter the bond vectors and thus the hopping parameters. Therefore, we also study the effect of strain on the electronic properties of SWCNs. Under both uniaxial and torsional strain, semiconductor–metal–semiconductor (S–M–S) phase transitions have been expected on primary metallic nanotubes.

We adopt the usual sp^3 tight-binding model together with nearest-neighbouring interactions to consider the σ–π hybridization of SWCNs. In terms of the rotational and helical symmetry of a SWCN, we need only consider a two-carbon-atom (A- and B-type) unit cell, defined by the dotted rhombus in figure 1(a). Eight Bloch orbitals, consisting of A and B atoms, constitute the basis functions, given by [19, 20]

$$\Phi_{j,\alpha}(r) = \frac{1}{\sqrt{N}} \sum_{R} \mathrm{e}^{\mathrm{i}\boldsymbol{K}\cdot\boldsymbol{R}} \varphi_j^{\alpha}(\boldsymbol{r} - \boldsymbol{R}), \qquad (\alpha = \text{A and B}) \tag{1}$$

where $\boldsymbol{K}$ is the wavevector. The summation is taken over the coordinate $\boldsymbol{R}$ for the A and B atoms, and φ_j denotes the atomic wavefunction in state j (j represents the 2s, $2p_x$, $2p_y$ and $2p_z$ orbitals). The eigenfunctions Ψ_j are then expressed as $\Psi_j = \sum_{j,\alpha} C_{j,\alpha} \Phi_{j,\alpha}(r)$, where $C_{j,\alpha}$ are components of the eigenvector of the Hamiltonian matrix $\boldsymbol{H}$. In the Slater–Koster scheme [19], $\boldsymbol{H}$ is written as [20]

$$\boldsymbol{H} = \begin{pmatrix} \boldsymbol{H}^{\mathrm{AA}} & \boldsymbol{H}^{\mathrm{AB}} \\ \boldsymbol{H}^{\mathrm{BA}} & \boldsymbol{H}^{\mathrm{BB}} \end{pmatrix}, \tag{2}$$

where $\boldsymbol{H}^{\mathrm{BA}} = (\boldsymbol{H}^{\mathrm{AB}})^*$. Since atoms A and B are really alike, $\boldsymbol{H}^{\mathrm{AA}}$ and $\boldsymbol{H}^{\mathrm{BB}}$ are the same 4×4 diagonal submatrices, of which four diagonal elements are determined by the s- and p-orbital energies of atoms. $\boldsymbol{H}^{\mathrm{AB}}$ is the interaction submatrix between atoms A and B. The main problem in predicting the effects of curvature on the electronic properties of SWCNs with curved surfaces has been determining accurately the matrix elements $\boldsymbol{H}^{\mathrm{AB}}_{jj'}(r_i)$, defined by [20],

$$\boldsymbol{H}^{\mathrm{AB}}_{jj'}(r_i) = \sum_{i} \mathrm{e}^{\mathrm{i}\boldsymbol{K}\cdot\boldsymbol{r}_i} f(d_i) \langle \varphi_j^{\mathrm{A}}(\boldsymbol{R}_{\mathrm{A}}) | \boldsymbol{H} | \varphi_{j'}^{\mathrm{B}}(\boldsymbol{R}_{\mathrm{A}} + \boldsymbol{r}_i) \rangle, \tag{3}$$

where $\boldsymbol{r}_i = \boldsymbol{R}_{\mathrm{B}} - \boldsymbol{R}_{\mathrm{A}}$ and $d_i = |\boldsymbol{r}_i|$. Here, to consider simultaneously the variation in bond length, the right-hand side of equation (3) is multiplied by a factor $f(d_i)$, which is usually given by the Harrison formula [10–13]. However, the d^{-2} dependence of the formula is invalid both at much larger atomic separation d and at the limit $d \to 0$, since the transfer integrals—together with the atomic wavefunction—fall off exponentially at the former limit and tend to a finite value of the on-site energy at the latter limit [10, 21]. In terms of the analytical formula of the transfer integral for the He molecule [21], we may assume that

$$f(d) = (1 + \lambda d)\mathrm{e}^{-\lambda(d - d_0)}/(1 + \lambda d_0), \tag{4}$$

where λ is a fitting parameter and d_0 is the equilibrium lattice separation. Equation (4) can describe the variations in transfer integrals under much larger and very small atomic separation, such as in the case of high strain. It is found that, at $\lambda d_0 = 2.732$, $f(d)$ has almost the same behaviour as the Harrison formula near d_0. Additionally, local density-functional calculations [1] have shown that one π-orbital per carbon atom is orientated normal to the tube

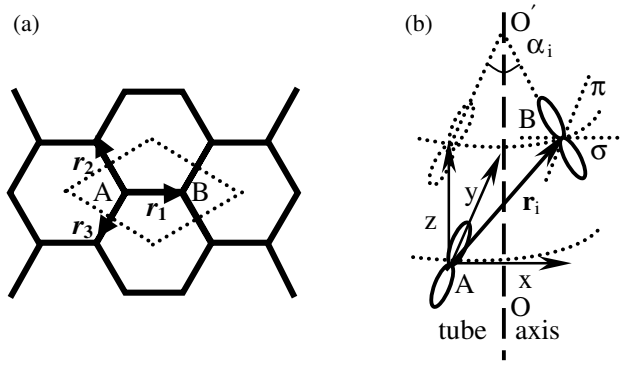

Figure 1. (a) An unrolled two-dimensional graphite sheet lattice. A two-carbon-atom unit cell is shown in the dotted rhombus. (b) A schematic of the relative positions of two nearest-neighbouring carbon atoms on the curved surface of a SWCNs along the r_i direction. The dashed line OO′ runs along the direction of the tube's axis.

surface. Thus, a rotational angle α_i exists between two neighbouring π orbitals along r_i on the surface of a SWCN [4, 6] (see figure 1(b)). The misalignment angle (half of the angle α_i) plays an important role in determining the curvature-induced gaps as a function of chirality and curvature [4–6]. Usually, the effect of variations in rotational angle on the electronic properties is neglected in a regular hybridization calculation. To take it into account, the wavefunctions of $|2p_x^B\rangle$ and $|2p_y^B\rangle$ are decomposed into their σ and π components in the directions parallel or perpendicular to the x-axis (see figure 1(b)), given by [20]

$$\begin{aligned} |2p_x^B\rangle &= \cos\alpha_i|2p_\sigma\rangle + \sin\alpha_i|2p_\pi\rangle, \\ |2p_y^B\rangle &= \cos\alpha_i|2p_\pi\rangle - \sin\alpha_i|2p_\sigma\rangle. \end{aligned} \tag{5}$$

The overlap integrals in equation (3) referring to φ_x^B and φ_y^B are then derived from

$$\begin{aligned} \langle\varphi_j^A|H|\varphi_x^B\rangle &= \cos\alpha_i E_{jx}(r_i) + \sin\alpha_i E_{jy}(r_i), \\ \langle\varphi_j^A|H|\varphi_y^B\rangle &= \cos\alpha_i E_{jy}(r_i) - \sin\alpha_i E_{jx}(r_i), \end{aligned} \tag{6}$$

where $E_{jj'}$ can be obtained directly from Slater–Koster tables [19, 23], which are dependent on the direction cosines (l_i, m_i, n_i) of the position vector r_i. Other overlap integrals in equation (3), independent of α_i, have the same forms as those in the Slater–Koster tables [19]. This decomposition can be used to describe a bond in any general direction, which is useful for fullerene-based structures with curved surfaces [20]. When evaluating the interactions between the A and B sublattice, only the three nearest-neighbouring terms in equation (3) are nonvanishing, since there are three B neighbours for an A site. Unlike in hexagonal graphite, the three σ-bonds are not in the same plane but are instead directed towards the positions of the nearest-neighbouring carbon atoms with the direction cosines (l_i, m_i, n_i), so the sum in equation (3) is usually nonzero. As a result, the states of the A and B sites in the curved surface indeed mix, due to the curvature, which leads to the rehybridization of σ- and π-states under our consideration. Once the matrix elements for the Bloch orbitals between the A and B atoms are given, the band structures can be obtained by solving the secular equation $\det[\boldsymbol{H} - E] = 0$ with eigen-energy E. The calculated band structures have then incorporated the main intrinsic curvatures in the curved surface of SWCNs.

We have used our model to calculate the band structures and band gaps of various types of SWCNs. The on-site energies and overlap integrals were taken from previous works [22, 23]

and were adjusted to fit the first-principle electronic structure results and the experimentally measured band gaps for fullerence tubes [6–9]. We used $E_s = -7.3$ and $E_p = 0.0$ eV for the on-site energies and $V_{ss\sigma} = -4.30$ eV, $V_{sp\sigma} = 4.98$ eV, $V_{pp\sigma} = 5.86$ eV and $V_{pp\pi} = -2.67$ eV for the nearest-neighbour interactions. Figure 2 depicts the calculated band gaps for different types of zigzag-type tube and armchair-type tube. For a comparison, the experimental data measured by three groups [6–8] are also included. Good agreement between theory and experiment is seen from figure 2(a). To explore the relative importance of various intrinsic curvatures, the dependence of band gaps on bond length, bond angle and regular hybridization is studied by varying each independently of the others. The regular σ–π hybridization calculation can be performed by assuming $f(d_i) = 1$ and $\alpha_i = 0$ in equations (3) and (6). Based on the single-π orbital model [4, 5], on the other hand, a straightforward analysis of the dependence of band gaps on variations in bond length can be obtained from equation (4) in terms of $\gamma_i = \gamma_0 f(d_i)$, where $\gamma_0 = |V_{pp\pi}|$. Also, the bond-angle dependence of band gaps may be discussed, provided that the single-parameter γ_i in the tight-binding approximation is defined to be $\gamma_i = \cos\alpha_i E_{yy} - \sin\alpha_i E_{xy}$, where $f(d_i) = 1$. As an example, the band gaps of primary metallic zigzag-type tubes are presented in figure 2(b). In all of the three cases, by only considering one type of curvatures one may observe the curvature-induced band gaps. It shows that each of the three main intrinsic curvatures has a contribution of varying importance to the band gaps, especially for a small-diameter nanotube. Next, the band gaps are under-estimated in all these cases, compared with the theoretical and experimental results. Therefore, a combination of the main intrinsic curvatures should be fully taken into account to discuss the underlying physics in fullerene-based structures with curved surfaces. Although one may additionally adjust the interacting parameters to fit the experimental data in the three cases, this may lead to a significant variation in the transfer integral γ_0. This result may help to explain the large deviations in γ_0 that were determined from different experiments, ranging from 2.45 to 3.20 eV [5–8, 11, 24].

We now explore the effect of strain on the electronic properties of SWCNs. In the framework of elasticity theory, the deformation can be written as [5, 11, 13] $\boldsymbol{r}_i' = (\boldsymbol{I} + \varepsilon)\boldsymbol{r}_i$, where $\boldsymbol{I}$ is the unit matrix, $\boldsymbol{r}_i'$ is the position vector of atom i after stress, and ε is given by

$$\varepsilon = \begin{pmatrix} \varepsilon_c & \xi \\ 0 & \varepsilon_t \end{pmatrix}, \tag{7}$$

where $\xi = \tan(\gamma)$ and γ is the shear strain. $\varepsilon_c = s_{12}\sigma$ and $\varepsilon_t = s_{11}\sigma$ are uniaxial strains along the circumferential and tube axial directions under both uniaxial traction ($\sigma > 0$) and compression ($\sigma < 0$), respectively [11].

The position of atoms after stress is determined by using the chirality-dependent coordinate system [12]. The graphite values $s_{11} = 0.98 \times 10^{-12} P_a^{-1}$, $s_{12} = -0.16 \times 10^{-12} P_a^{-1}$ [11] are used in our work. We still focus on the primary metallic tubes. The band gap and the band structure near the Fermi energy can be obtained by finding the minimum of the lowest-lying conduction band and the maximum of the highest-lying valence band [4].

Under a uniaxial stresses with $\xi = 0$, the results are given in figure 3. The band gaps at zero stress can be fitted well to the experimental data [6]. This may ensure the reliability of the comparison between theory and experiment. From figure 3, S–M–S transitions are observed for primary metallic non-armchair nanotubes, while the application of uniaxial strain does not cause a band gap for an armchair tube, which is consistent with previous works [11–13]. The critical stress σ_c of the transition corresponds to a truncation ($0 < \sigma_c < 20$ GPa) other than a compression ($\sigma < 0$; see [11]), which is less than an average breaking strength (30 GPa; see [14]). Thus, the transitions are observable experimentally. Using a more detailed analysis, it is found that the gap sensitivity with stress $\mathrm{d}E_g/\mathrm{d}\sigma$ shows a small difference between the

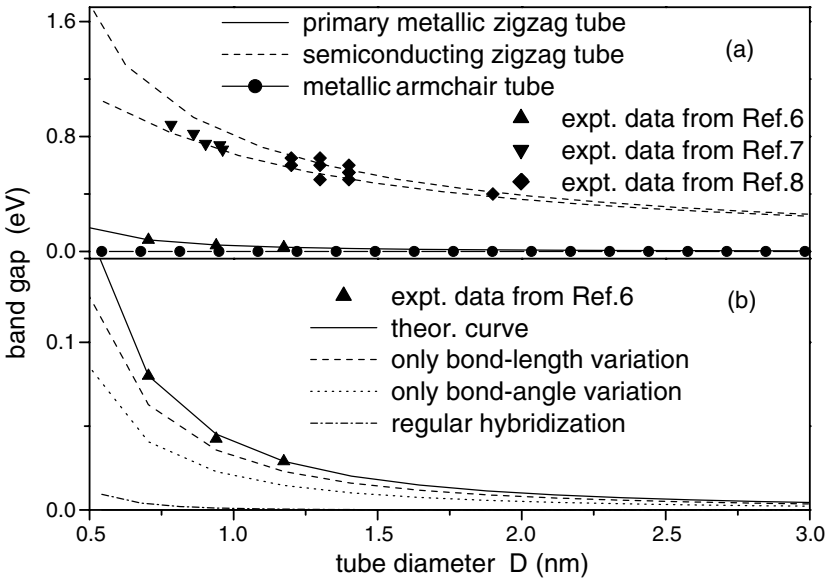

Figure 2. (a) The theoretically calculated and experimentally measured band gaps of zigzag-type and armchair-type tubes. (b) The relative importance of the three main intrinsic curvatures on the induced band gaps of the primary metallic zigzag-type tubes.

values before and after the transition, and the values of σ_c depend on both the diameter and the chirality of the nanotubes. For example, the value of $|dE_g/d\sigma|$ for the (9, 0) tube is 9.81 meV GPa^{-1} at $\sigma < \sigma_c \approx 10$ GPa, but 8.52 meV GPa^{-1} at $\sigma > \sigma_c$. This is at variance with previous predictions [11–13].

When considering the changes in bond lengths by using the Harrison formula, we also calculate the band gaps of the (9, 0) tube (see the dotted line in figure 3). As expected, the difference in band gaps is almost unobservable between the two cases of the Harrison formula and equation (4). However, an observable change appears under high strain. The band gap and its sensitivity with stress decrease at $\sigma > \sigma_c$ but increase at $\sigma < \sigma_c$. This shows that the Harrison formula should be amended to obtain the band structure accurately at much larger d and at the limit $d \to 0$. Perhaps this indicates that the present model and the method may be more useful for the tight-binding computation of the scanning tunnelling microscopy (STM) image [22], where the separation between the sample and the tip of the STM is much larger than the lattice constant.

In the case of a small torsional strain with $\sigma = 0$, S–M–S transitions are also found in armchair-type and chiral tubes, as shown in figure 4. It further shows that a twist deformation is the only possible source for a band gap in an armchair-type tube [5, 12, 13]. It is due to the curvature-induced band gap at zero strain that the 'V'-shaped curve for a chiral tube is shifted away from the origin. For a zigzag-type tube with small tube diameter, the band gap decreases as the shear strain increases, but no transition appears. As the tube diameter increases, interestingly a symmetrical 'W'-shaped curve emerges for the band gap as a function of torsional strain (see figure 4). Thus the S–M–S transition can be observed at both positive and negative critical torsional strain. This may be related to the high symmetry of a zigzag-type tube. Therefore, primary metallic zigzag-type tubes are very sensitive to torsional strain. The result is different from the previous

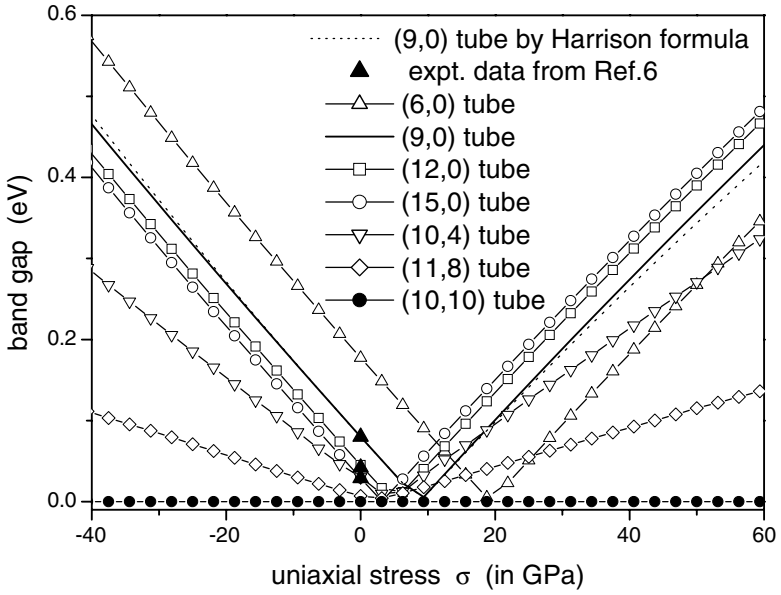

Figure 3. Band gap versus uniaxial strain for various types of primary metallic nanotubes. The dotted line corresponds to the band gap of a (9, 0) tube with the bond-length changes according to the Harrison formula.

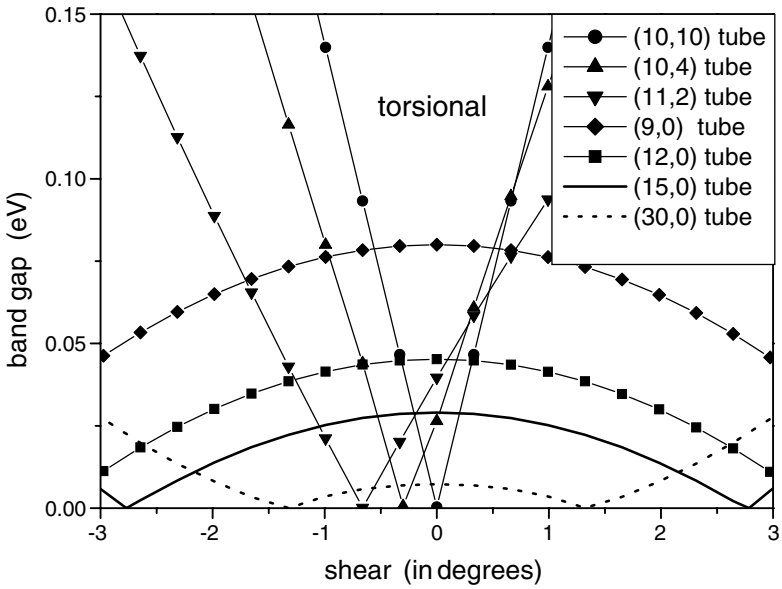

Figure 4. Band gap versus torsional strain for various types of primary metallic nanotubes.

works [11–13]. In terms of the deformation-tuned properties of nanotubes, therefore, one can manipulate the electronic properties of SWCNs at will by developing the art of nano-mechanic technology [14]. This may provide an alternative way to explore the intrinsic electronic properties of SWCNs.

This work is supported by the National Natural Science Foundation of China under Grant Nos 10074052 and 10005007, the National 973 Project of China under Grant No 1999-0645-4500, the Mid-youth Science-technology Foundation of Hunan Province under Grant No 00JZY2138, and the Provincial Natural Science Foundation of Hunan, China under Grant No 01JJY2002.

References

[1] Blase X *et al* 1994 *Phys. Rev. Lett.* **72** 1878
[2] Kleiner A *et al* 2001 *Phys. Rev.* B **64** 113–402
[3] Chen P *et al* 1999 *Phys. Rev. Lett.* **82** 2548
[4] Ding J W, Yan X H and Cao J X 2002 *Phys. Rev.* B **66** 073401
[5] Kleiner A *et al* 2001 *Phys. Rev.* B **63** 073408
[6] Ouyang M *et al* 2001 *Science* **292** 702
[7] Odom T W *et al* 1998 *Nature* **391** 62
[8] WildÖer J W G *et al* 1998 *Nature* **391** 59
[9] Zhou C *et al* 2000 *Phys. Rev. Lett.* **84** 5604
[10] Froyen S and Harrison W A 1979 *Phys. Rev.* B **20** 2420
Harrison W A 1981 *Phys. Rev.* B **24** 5835
[11] Heyd R, Charlier A and McRae E 1997 *Phys. Rev.* B **55** 6820
[12] Yang L *et al* 1999 *Phys. Rev.* B **60** 13874
[13] Yang L and Han J 2000 *Phys. Rev. Lett.* **85** 154
[14] Yu M F *et al* 2000 *Phys. Rev. Lett.* **84** 5552
[15] Lammert P E *et al* 2000 *Phys. Rev. Lett.* **84** 2453
[16] Rochefort A *et al* 1999 *Phys. Rev.* B **60** 13824
[17] Park C J *et al* 1999 *Phys. Rev.* B **60** 10656
[18] Yakobson B I *et al* 1996 *Phys. Rev. Lett.* **76** 2511
[19] Slater J C and Koster G F 1954 *Phys. Rev.* **94** 1498
[20] Saito R, Dresselhaus G and Dresselhaus M S 1998 *Physical Properties of Carbon Nanotubes* (London: Imperial College Press)
[21] Flügge S 1974 *Practical Quantum Mechanics* vol 1 (New York: Springer)
[22] Tomanek D and Louie S G 1988 *Phys. Rev.* B **37** 8327
[23] Cao J X, Yan X H, Ding J W and Wang D L 2001 *J. Phys.: Condens. Matter* **13** L271
[24] Saito R, Dresselhaus G and Dresselhaus M S 2000 *Phys. Rev.* B **61** 2981